

High magnetic field spin-valley-split Shubnikov–de Haas oscillations in a WSe₂ monolayer

Banan Kerdi^{1,*}, Mathieu Pierre¹, Robin Cours², Bénédicte Warot-Fonrose², Michel Goiran¹, and Walter Escoffier^{1,†}

¹LNCMI, Université de Toulouse, CNRS, INSA, UPS, EMFL, 31400 Toulouse, France

²CEMES, Université de Toulouse, CNRS, 31055 Toulouse, France

We study Shubnikov–de Haas oscillations in a p-type WSe₂ monolayer under very high magnetic field. The oscillation pattern is complex due to a large spin and valley splitting, in the non-fully-resolved Landau level regime. Our experimental data can be reproduced with a model in which the main parameter is the ratio between the Zeeman energy and the cyclotron energy. The model takes into account the Landau levels from both valleys with the same Gaussian broadening, which allows to predict the relative amplitude of the resistance oscillation originating from each valley. The Zeeman energy is found to be several times larger than the cyclotron energy. It translates into a large and increasing effective Landé factor as the hole density decreases, in the continuity of the values reported in the literature at lower carrier density.

I. INTRODUCTION

Single atomic layers of semiconducting transition metal dichalcogenides (TMDCs) have received much attention over the last decade due to their promising characteristics for two-dimensional-based (2D) optoelectronic devices [1–4] and their potential for the development of valleytronics physics [5]. The crystal structure of these 2D materials, composed of one transition metal atom (W, Mo) and two chalcogen atoms (S, Se) per unit cell arranged in a honeycomb lattice, leads to a direct band gap in the visible range, located at the corner (K and K' points) of the first Brillouin zone [1, 2, 6]. The lack of inversion symmetry of the crystal structure, combined with strong spin-orbit coupling due to the heavy transition metal atoms, translate into coupled valley and spin degrees of freedom of the charge carriers, later referred to as the $|K \uparrow\rangle$ and $|K' \downarrow\rangle$ states. The presence of an out-of-plane magnetic field not only turns the energy spectrum into discrete Landau levels (LL), separated by the cyclotron energy E_c , but also lifts the spin/valley degeneracy of the $|K \uparrow\rangle$ and $|K' \downarrow\rangle$ states through Zeeman energy $E_z = g^* \mu_B B$ where μ_B is the Bohr magneton and g^* is the effective Landé factor. In TMDC monolayers, experimental studies point to a very large value of g^* since the spin, orbital, and lattice Zeeman effects add up to each other [7–9]. The first effect refers to the interaction between the magnetic field and the electron or hole spin, the second is linked to the spin-orbit coupling, and the last alludes to the opposite Berry curvatures in the non-equivalent K and K' valleys [10]. While the effective Landé factor of excitons in TMDC monolayers has been measured by several groups [11–14], it would be desirable to obtain this fundamental parameter for the conduction and valence bands independently. g^* is expected to depend on the chemical composition and the number of

layers of the TMDC, on the nature (electron or hole) of the charge carriers, as well as the carrier density. In this work, we focus on its determination for holes in WSe₂ monolayers, which we extend to high carrier concentration thanks to a very high magnetic field.

In general, the ratio E_z/E_c , from which g^* is extracted, can take any value, leading to non-equidistant Landau levels and complex Shubnikov–de Haas (SdH) oscillations in a magneto-transport experiment. Figure 1 shows the Landau level spectrum as a function of magnetic field in the case of a large spin-valley splitting (Fig. 1a) and its evolution with E_z/E_c (Fig. 1b). When this ratio is not an integer, the non-equidistant Landau levels translate into non $1/B$ -periodic quantum oscillations, as illustrated in Fig. 1c. In 2D electron gases (2DEG) realized in standard semiconducting heterostructures, the effective Landé factor is experimentally addressed by tilting the magnetic field with respect to the sample's plane. Indeed, the Zeeman energy E_z depends on the magnetic field intensity regardless of its orientation whereas the cyclotron energy E_c is proportional to the out-of-plane projection of the magnetic field. A coincidence angle is reached when the Zeeman energy equals the cyclotron energy, and the magneto-resistance recovers the distinctive $1/B$ -periodicity of single-carrier Shubnikov–de Haas oscillations. In the case of TMDCs, however, this coincidence method fails because the spin of the charge carriers is locked to the sample's out-of-plane direction [9, 15]. Nonetheless, and beyond the difficulty in obtaining high-mobility samples with low-resistance ohmic contacts, a few studies have reported the ratio E_z/E_c based on the analysis of SdH oscillations. In Ref. 9, an estimation of E_z/E_c rounded to integer values has been extracted from sequences of SdH oscillation minima at odd or even filling factors. In Ref. 16, the identification of the transition between mixed and polarized Landau level regimes has been exploited to deduce an electron-density dependent g^* factor in high-mobility MoS₂ bilayers. Otherwise, as an alternative to magneto-transport, contactless spectroscopy using a single-electron transistor has been

* banan.kerdi@lncmi.cnrs.fr

† walter.escoffier@lncmi.cnrs.fr

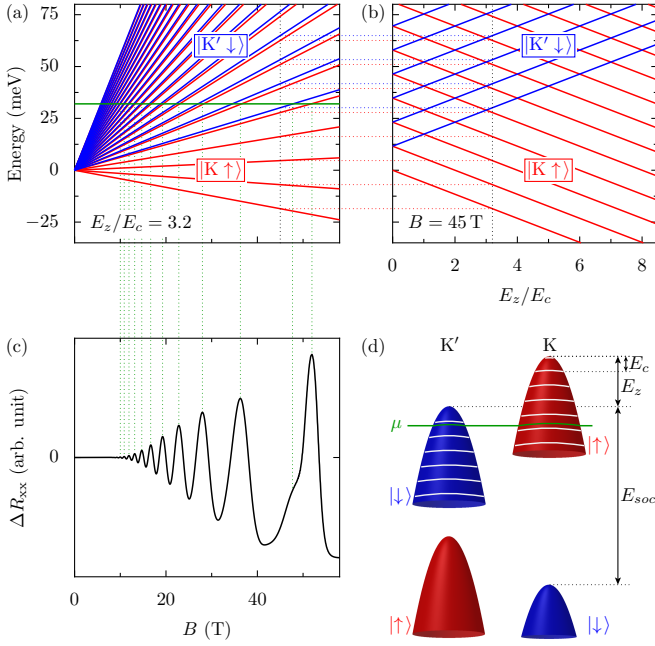


FIG. 1. Energy of LLs as a function of (a) magnetic field and (b) E_z/E_c where the red and blue lines represent the $|K \uparrow\rangle$ and $|K' \downarrow\rangle$ states, respectively. (c) Simulated magneto-resistance where both a large LL broadening and a non-integer ratio $E_z/E_c = 3.2$ have been chosen to produce an example of complex oscillations. The simulation is performed at constant chemical potential corresponding to the solid green line depicted in panel (a). A maximum of resistance is expected each time the chemical potential crosses a LL. (d) Simplified valence band of WSe₂ monolayers under magnetic field. The valleys at points K and K' of the first Brillouin zone are made of two spin-split parabolic bands. For a given spin sign, the energy difference between the two bands arises from the spin-orbit coupling (SOC), with $E_{\text{soc}} = 466$ meV [17, 18]. The white lines indicate the energies of the Landau levels for $E_z/E_c = 3.2$. They are shown only for the two upper bands, where the chemical potential (solid green line) is located in the explored range of hole densities.

used to sense directly the chemical potential and infer the Landau level spectrum [8].

In this work, we performed magneto-transport measurement in a WSe₂ monolayer under very high magnetic field, allowing for partial Landau level resolution in samples with reasonable mobilities fabricated without complicated contact engineering. We analyze the complex SdH oscillation pattern using a model where E_z/E_c is the main fitting parameter. It takes into account all the $|K \uparrow\rangle$ and $|K' \downarrow\rangle$ Landau levels at once with the same Gaussian broadening. This novel approach is particularly helpful to analyze oscillations with non-fully-resolved spin and valley splitting.

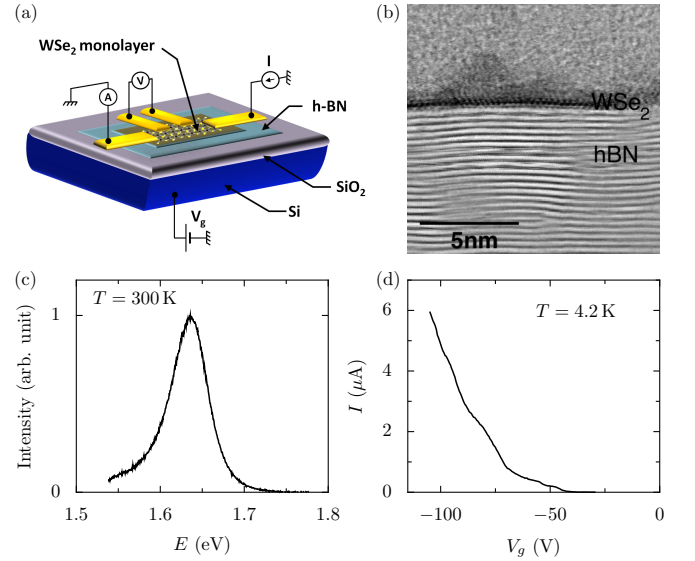


FIG. 2. (a) Sketch of the BN/WSe₂ heterostructure. (b) Bright-field scanning transmission electron microscopy (BF-STEM) image realized after the measurement campaign confirming a WSe₂ monolayer as the conducting channel. The h-BN substrate appears as dark/bright fringes whereas the WSe₂ layer consists of dark spots surrounded by brighter ones. The interatomic distances between W and Se atoms correspond to the expected ones. (c) The photoluminescence spectrum with $\lambda_{\text{exc}} = 633$ nm is characteristic of a WSe₂ monolayer. (d) Current flowing in the device for $V_{ds} = 100$ mV versus the back-gate voltage.

II. EXPERIMENTS

A single atomic layer of WSe₂ is exfoliated from the bulk material [19] using the micro-mechanical cleavage method and transferred onto a stamp of PDMS [20]. This flake is deposited under optical microscope control onto a 20-nm-thick flake of Boron Nitride (BN) pre-deposited on a standard Si/SiO₂ substrate with $d_{\text{SiO}_2} = 280$ nm. Electron beam lithography with a 495 K (100 nm)/950 K (80 nm) PMMA bilayer mask followed by platinum sputtering (10 nm) and gold thermal evaporation (50 nm), is realized to fabricate the electrodes, as sketched in Fig. 2a. The WSe₂ flake is later confirmed to be a monolayer by photoluminescence (Fig. 2c) and bright-field scanning transmission electron microscopy (Fig. 2b). In this transistor configuration, the back-gate voltage (V_g) applied between the sample and the substrate sets the hole density.

We performed transport measurements under pulsed magnetic field up to 54 T at low temperature (4.2 K) for different values of the back-gate voltage. A constant DC current of 1 μA is passed through the sample while the longitudinal voltage is measured during a pulse of magnetic field with total duration ~ 500 ms. The magneto-resistance displays large-amplitude oscillating features on top of a smooth background, subtracted to the data to obtain the oscillatory part $\Delta R_{xx}(B)$ of the signal only,

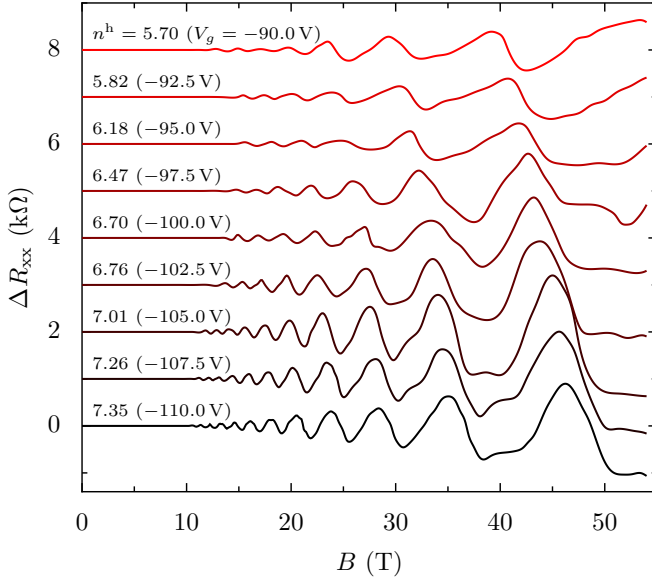


FIG. 3. High field magneto-resistance of the sample at $T = 4.2$ K, after background removal, for various values of the carrier density n^h (given in unit of 10^{12} cm^{-2}) ranging from 5.70 to $7.35 \times 10^{12} \text{ cm}^{-2}$. The corresponding back-gate voltage V_g is given in parentheses. An offset of $1 \text{ k}\Omega$ is set between consecutive curves for clarity. The strong deviations from a $1/B$ -periodic oscillatory behavior are indicative of an additional Zeeman energy scale competing with the cyclotron energy. See also Supplemental Material I where the same dataset is plotted versus filling factor.

as shown in Fig. 3. For all gate voltages, the oscillations exhibit a complex pattern, requiring an analysis beyond spin-degenerate single-band $1/B$ -periodic SdH oscillations. The large spin/valley splitting is responsible for this effect, as explained in the Introduction.

III. MODELING AND SIMULATIONS

To extract the ratio E_z/E_c , we performed numerical simulations of the oscillatory part of the resistance $\Delta R_{xx}(B)$. We start with the LL structure of WSe_2 , adapted from the massive Dirac fermion dispersion relation [21–23], which provides the set of energies $E_{N,s}$ at a given magnetic field B .

$$E_{N,s} = -N\hbar\omega_c - sg^*\mu_B B, \quad (1)$$

where $\omega_c = eB/m^*$ is the cyclotron energy, g^* is the effective Landé factor, $N = 0, 1, 2, \dots$ is the LL index, and $s = \pm \frac{1}{2}$ stands for the coupled spin/valley degree of freedom, respectively $|K \uparrow\rangle$ and $|K' \downarrow\rangle$. We set $s = +\frac{1}{2}$ for $N = 0$ to satisfy energy minimization argument [24]. Under quantizing magnetic field and assuming a finite energy relaxation time, the density of states can be described by a sum of area-normalized Gaussian functions

centered at the energy of the LLs $E_{N,s}$,

$$\text{DoS}(E, B) = \sum_{N,s} \frac{eB}{h} \times \frac{1}{\sqrt{2\pi}\Gamma(B)} \times \exp\left(-\frac{(E - E_{N,s})^2}{2\Gamma^2(B)}\right), \quad (2)$$

where $\Gamma(B) = \frac{\hbar e}{m^*} \sqrt{\frac{2B}{\pi\mu^h}}$ with μ^h the hole mobility at zero magnetic field [25]. The pre-factor eB/h accounts for the orbital degeneracy of the LLs. We assume that the charge density n^h remains constant in the device, set by the fixed back-gate voltage V_g , while the chemical potential changes according to the variation of the density of states at the Fermi energy induced by the magnetic field. For each value of the magnetic field, the chemical potential $\mu(B)$ is obtained numerically by solving

$$n^h = \int_{-\infty}^{+\infty} \text{DoS}(E, B) \times f(E, \mu(B), T) \times dE, \quad (3)$$

i.e., when the cumulative orbital degeneracy of the occupied LLs reaches the hole carrier density. Here, $f(E, \mu, T) = \frac{1}{1 + \exp\left(\frac{E - \mu}{k_B T}\right)}$ is the Fermi-Dirac distribution function. The conductivity $\sigma_{xx}(B)$ is calculated from [26]

$$\begin{aligned} \sigma_{xx}(B) &= \frac{e^2}{h} \sum_{N,s} \int_{-\infty}^{+\infty} \left(N + \frac{1}{2}\right) \\ &\times \left[\exp\left(-\frac{(E - E_{N,s})^2}{2\Gamma^2(B)}\right) \right]^2 \times \left[\frac{\partial f(E, \mu, T)}{\partial E} \right] \times dE. \end{aligned} \quad (4)$$

Here, the conductivity of the system is interpreted within the two-fluid model without interaction between the charge carriers belonging to different valley/spin indices. The contributions of each quantum state to the conductivity add therefore independently. We emphasize that this model is certainly oversimplified since it cannot reproduce LL anti-crossing as investigated in Refs. 16 and 27 for MoS_2 and Ref. 8 for WSe_2 . The longitudinal resistivity ρ_{xx} is computed by inverting the conductivity tensor, where the product $\sigma_{xx} \times \rho_{xy} \ll 1$ can be expanded in a Taylor series when the chemical potential is located in between two successive LLs. We obtain

$$\rho_{xx} = \sigma_{xx} \times \rho_{xy}^2 + \sigma_{xx}^3 \times \rho_{xy}^4 + \dots, \quad (5)$$

where the Hall resistivity ρ_{xy} is computed from the relation

$$\rho_{xy} = \frac{h}{e^2} \left[\int_{-\infty}^{+\infty} \sum_{N,s} \frac{dE}{\sqrt{2\pi}\Gamma(B)} \times \exp\left(-\frac{(E - E_{N,s})^2}{2\Gamma^2(B)}\right) \right]^{-1}. \quad (6)$$

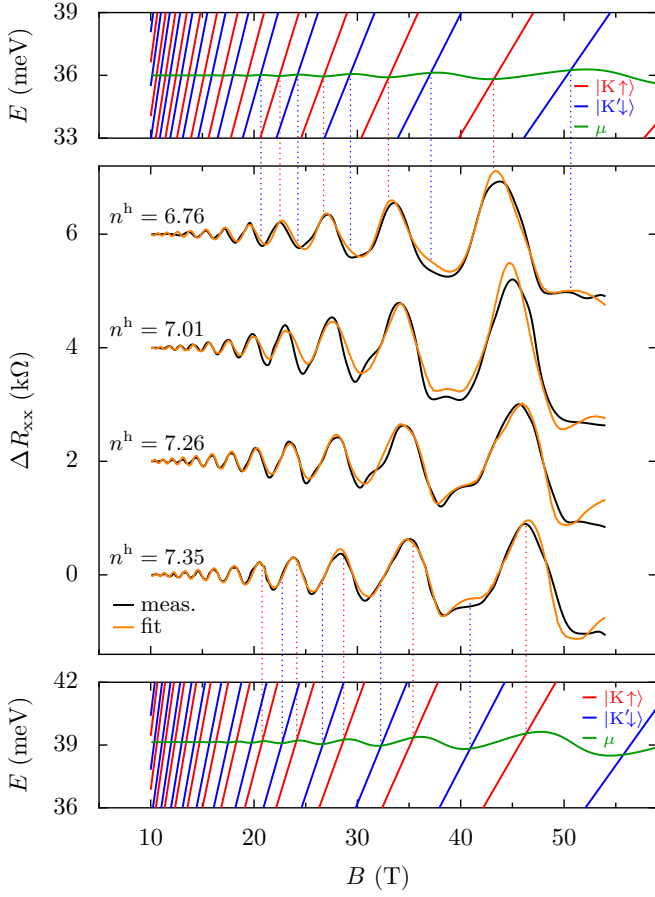


FIG. 4. Middle frame: The experimental magneto-resistance (black lines) are compared to the model output (orange lines) for selected hole densities n^h (given in unit of 10^{12} cm^{-2}). Top and bottom frames: Landau level spectrum and evolution of the chemical potential $\mu(B)$ for $n^h = 6.76 \times 10^{12} \text{ cm}^{-2}$ and $n^h = 7.35 \times 10^{12} \text{ cm}^{-2}$, respectively. Deviations from $1/B$ -periodic oscillations appear at high field, as a direct consequence of the non-integer E_z/E_c ratio. See also Supplemental Material II for additional fits of the data.

Despite some mismatch in the relative amplitude of the oscillations, probably linked to imprecise background subtraction, the overall shape of the curves is nicely reproduced without invoking any change of E_z/E_c with magnetic field (see Fig. 4). The best fits provide the hole density n^h , the mobility μ^h and the ratio E_z/E_c . We used the same mobility for the $|K \uparrow\rangle$ and $|K' \downarrow\rangle$ states as we suppose that the main sources of scattering (remote charged impurities and punctual lattice defects) are spin/valley independent. The effective mass is set to $m^* = 0.45 \times m_e$ where m_e is the bare electron mass (see Supplemental Material IV) and the temperature is set constant at $T = 4.2 \text{ K}$. The numerical simulation also includes the optimization of the mobility edge, which sets the energy threshold between localized and extended states in LLs, as a magnetic field-dependent cut-off of the Gaussian functions in Eqs. (4) and (6). The extracted hole density with respect to V_g is in good agreement with the plane capacitor model (see

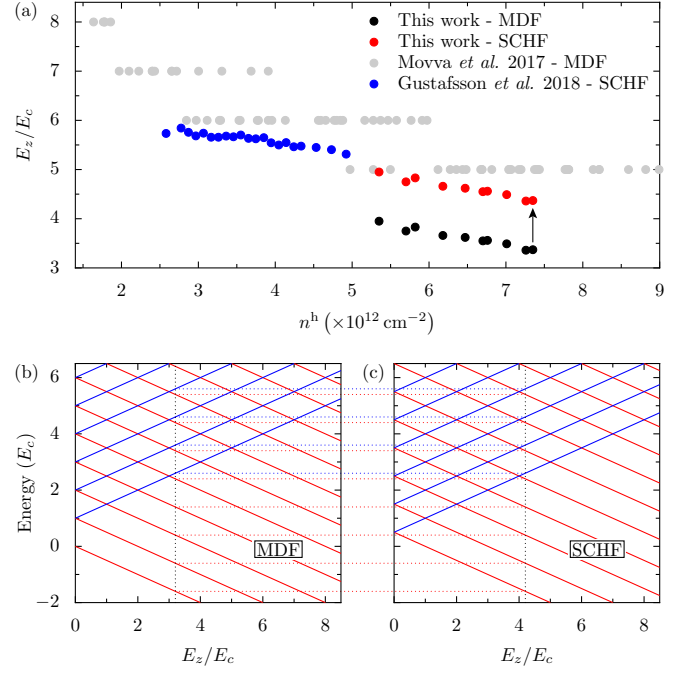


FIG. 5. (a) Extracted values of E_z/E_c as a function the hole density. The black dots are the values obtained assuming the Landau level structure of Massive Dirac Fermions (MDF). By up-shifting these values by 1, we obtain the values corresponding to the LL structure of Schrödinger Fermions (SCHF). E_z/E_c increases as the carrier density reduces, suggesting the reinforcement of the Coulomb interactions. The E_z/E_c ratio is compared to the values found in the literature (blue and gray dots), where either the MDF or SCHF model was considered (see main text). (b), (c) Comparison of LL energies in cyclotron energy unit as a function of E_z/E_c for the (b) MDF and (c) SCHF models. This figure demonstrates that their LL structure is identical under an up-shift of E_z/E_c by 1.

Supplemental Material III) where the gate capacitance per unit area, $C_g = (C_{\text{SiO}_2}^{-1} + C_{\text{BN}}^{-1})^{-1} = 11.5 \text{ nF/cm}^2$, is derived from the SiO_2 thickness of 280 nm and the BN thickness of 20 nm with relative dielectric permittivity $\epsilon_r(\text{SiO}_2) = 3.9$ and $\epsilon_r(\text{BN}) = 3.8$, respectively. We obtain $\mu^h \sim 2000 \text{ cm}^2 \text{ V}^{-1} \text{ s}^{-1}$ for $n^h \gtrsim 6.5 \times 10^{12} \text{ cm}^{-2}$, with a progressive drop down to $\mu^h \sim 1000 \text{ cm}^2 \text{ V}^{-1} \text{ s}^{-1}$ as the hole density decreases. For $n^h < 5.7 \times 10^{12} \text{ cm}^{-2}$, the amplitude of the oscillations is too weak with respect to the magneto-resistance background, preventing a reliable determination of E_z/E_c .

IV. DISCUSSION

Our simulations suggest that the ratio E_z/E_c is comprised between 3 and 4 for $n^h = 7.5$ till $5 \times 10^{12} \text{ cm}^{-2}$, respectively (see black dots in Fig. 5a). To establish this result, we particularly focused on the specific shape of the high-field oscillations, as shown in Fig. 4. Although a shift of $-2, +2, +4, \dots$ on the ratio E_z/E_c gives the same

apparent splitting between the $|K \uparrow\rangle$ and $|K' \downarrow\rangle$ LLs (see Fig. 1b), the simulated SdH oscillation pattern turns out different at high field. Indeed, the amplitude of the conductivity depends on the LL index [25] in Eq. (4). Therefore, the relative amplitude of the resistance peaks corresponding to the crossings of $|K \uparrow\rangle$ and $|K' \downarrow\rangle$ LLs with the chemical potential varies according to the exact value of E_z/E_c . Moreover, the system is expected to undergo a transition from a mixed to a polarized LL regime at a critical field depending on E_z/E_c . In this study, no hint of such a transition could be clearly identified. Nevertheless, it is possible to set a higher limit on E_z/E_c . For instance, for $V_g = -97.5$ V (see Supplemental Material II), we observe a low-amplitude resistance peak at 49 T which we attribute to the crossing of the chemical potential with a $|K' \downarrow\rangle$ LL. For this gate voltage, the best fit gave $E_z/E_c = 3.58$. If this ratio was offset by +2, an additional large amplitude peak corresponding to a $|K \uparrow\rangle$ LL should be observed instead, indicating that the transition would occur within our experimental magnetic field range. A similar conclusion can be drawn for all gate voltages ≥ -100 V, ruling out values of E_z/E_c above ~ 4 in the explored range of hole densities.

Figure 5a compares our results to those of Movva *et al.* [9] and Gustafsson *et al.* [8] marked by gray and blue dots, respectively. In the first study, the E_z/E_c ratio takes integer values only, since the authors detected the magneto-resistance minima at even(odd)-integer values of the filling factor corresponding to odd(even)-integer E_z/E_c ratio [28]. In the second study, however, the E_z/E_c ratio is determined from the chemical potential jumps between successive LLs, detected using a single-electron transistor coupled to the WSe₂ monolayer. Interestingly, the authors assumed a LL structure based on a Schrödinger Fermion (SCHF) model. Compared to the massive Dirac Fermion (MDF) model and regarding transport properties only, the main difference lies in the double spin/valley degeneracy of the 0th Landau level for $E_z = 0$. In systems where the Zeeman energy is very weak compared to the LL gap, this difference translates into a shift of the SdH oscillations by half a period. This effect has been particularly put forward in graphene to distinguish its peculiar electronic properties (originating from massless Dirac fermions) from those of standard semiconducting 2DEG [29, 30]. However, for systems such as TMDCs where E_z can be several times larger than E_c , the distinction between the two models is uncertain. Indeed, our experimental data could be fitted in a similar way considering the SCHF model with the ratio E_z/E_c up-shifted by 1 (see Figs. 5b and 5c). Although our study provides the value of E_z/E_c plus or minus 1 depending on the fermion model, it is noteworthy that its variation versus n^h shows the same slope compared to the few data available in the literature.

V. CONCLUSION

To conclude, we studied the Zeeman-effect-dependent magneto-resistance oscillation pattern of a WSe₂ monolayer sample under strong magnetic field at low temperature. The chemical potential lies in the valence band and the explored range of hole density ranges from 7.5 till $5 \times 10^{12} \text{ cm}^{-2}$. The high carrier density prevents the observation of the transition from the mixed to the polarized LL regime. However, the special shape of the quantum oscillations, which deviates from perfect $1/B$ -periodicity, is a clear signature of partially overlapping LLs from the $|K \uparrow\rangle$ and $|K' \downarrow\rangle$ states. These features are well reproduced using the Gaussian model for conductivity, with no interaction between charge carriers of opposite spins. We extract the ratio E_z/E_c , which increases as the hole density decreases, thereby enlarging the carrier density range where the enhancement of g^* has been reported. For systems with negligible Zeeman energy, the magneto-transport technique is sensitive to the degeneracy of the 0th LL and therefore allows a distinction between the LL structure originating from Dirac or Schrödinger fermions. Here, a large Zeeman energy prevents an unambiguous determination of E_z/E_c , as the fermion type in TMDC monolayers is still controversial. In this case, this ratio is inferred ± 1 depending on the fermion model, but cannot be larger than ~ 5 in the present study and within the experimentally accessible range of hole density. The ratio E_z/E_c is directly linked to the effective g -factor $g^* = \frac{2m_e}{m^*} \times \frac{E_z}{E_c}$, which ranges between 14.7 and 17.3 for $3.3 < E_z/E_c < 3.9$ and from 19.1 to 21.8 for $4.3 < E_z/E_c < 4.9$, considering a fixed effective mass ($m^* = 0.45 \times m_e$) of the holes.

ACKNOWLEDGMENTS

We acknowledge funding from ANR under project MoS₂ValleyControl No. ANR-14-CE26-0017 and financial support through the EUR grant NanoX No. ANR-17-EURE-0009 in the framework of the “Programme des Investissements d’Avenir”. The high magnetic field measurements were performed at LNCMI-Toulouse under EMFL proposals TSC01-118 and TSC07-218. We thank Emmanuel Courtade, Cédric Robert, and their colleagues at LPCNO and Pascal Puech (CEMES) for performing room-temperature photoluminescence characterization of our samples; Thomas Blon (LPCNO) for providing access to a metallic thin-film deposition machine; and our technical staff colleagues at LNCMI-Toulouse.

-
- [1] A. Splendiani, L. Sun, Y. Zhang, T. Li, J. Kim, C.-Y. Chim, G. Galli, and F. Wang, *Nano Letters* **10**, 1271 (2010).
- [2] K. F. Mak, C. Lee, J. Hone, J. Shan, and T. F. Heinz, *Physical Review Letters* **105**, 136805 (2010).
- [3] Z. Yin, H. Li, H. Li, L. Jiang, Y. Shi, Y. Sun, G. Lu, Q. Zhang, X. Chen, and H. Zhang, *ACS Nano* **6**, 74 (2012).
- [4] O. Lopez-Sanchez, D. Lembke, M. Kayci, A. Radenovic, and A. Kis, *Nature Nanotechnology* **8**, 497 (2013).
- [5] D. Xiao, G. B. Liu, W. X. Feng, X. D. Xu, and W. Yao, *Physical Review Letters* **108**, 196802 (2012).
- [6] W. Zhao, Z. Ghorannevis, L. Chu, M. Toh, C. Kloc, P.-H. Tan, and G. Eda, *ACS Nano* **7**, 791 (2013).
- [7] R. Pisoni, A. Kormanyos, M. Brooks, Z. J. Lei, P. Back, M. Eich, H. Overweg, Y. Lee, P. Rickhaus, K. Watanabe, T. Taniguchi, A. Imamoglu, G. Burkard, T. Ihn, and K. Ensslin, *Physical Review Letters* **121**, 247701 (2018).
- [8] M. V. Gustafsson, M. Yankowitz, C. Forsythe, D. Rhodes, K. Watanabe, T. Taniguchi, J. Hone, X. Y. Zhu, and C. R. Dean, *Nature Materials* **17**, 411 (2018).
- [9] H. C. P. Movva, B. Fallahazad, K. Kim, S. Larentis, T. Taniguchi, K. Watanabe, S. K. Banerjee, and E. Tutuc, *Physical Review Letters* **118**, 247701 (2017).
- [10] G. Aivazian, Z. Gong, A. M. Jones, R.-L. Chu, J. Yan, D. G. Mandrus, C. Zhang, D. Cobden, W. Yao, and X. Xu, *Nature Physics* **11**, 148 (2015).
- [11] A. A. Mitioglu, P. Plochocka, Á. Granados del Aguila, P. C. M. Christianen, G. Deligeorgis, S. Anghel, L. Kulyuk, and D. K. Maude, *Nano Letters* **15**, 4387 (2015).
- [12] A. V. Stier, K. M. McCreary, B. T. Jonker, J. Kono, and S. A. Crooker, *Nature Communications* **7**, 10643 (2016).
- [13] M. Koperski, M. R. Molas, A. Arora, K. Nogajewski, M. Bartos, J. Wyzula, D. Vaclavkova, P. Kossacki, and M. Potemski, *2D Materials* **6**, 015001 (2018).
- [14] M. Goryca, J. Li, A. V. Stier, T. Taniguchi, K. Watanabe, E. Courtade, S. Shree, C. Robert, B. Urbaszek, X. Marie, and S. A. Crooker, *Nature Communications* **10**, 4172 (2019).
- [15] Z. Y. Zhu, Y. C. Cheng, and U. Schwingenschlogl, *Physical Review B* **84**, 153402 (2011).
- [16] J. Lin, T. Han, B. A. Piot, Z. Wu, S. Xu, G. Long, L. An, P. Cheung, P. P. Zheng, P. Plochocka, X. Dai, D. K. Maude, F. Zhang, and N. Wang, *Nano Letters* **19**, 1736 (2019).
- [17] G.-B. Liu, W.-Y. Shan, Y. Yao, W. Yao, and D. Xiao, *Physical Review B* **88**, 085433 (2013).
- [18] D. Le, A. Barinov, E. Preciado, M. Isarraraz, I. Tanabe, T. Komesu, C. Troha, L. Bartels, T. S. Rahman, and P. A. Dowben, *Journal of Physics: Condensed Matter* **27**, 182201 (2015).
- [19] The WSe₂ bulk crystal has been bought from 2Dsemiconductors. (www.2dsemiconductors.com)
- [20] A. Castellanos-Gomez, M. Buscema, R. Molenaar, V. Singh, L. Janssen, H. S. J. van der Zant, and G. A. Steele, *2D Materials* **1**, 011002 (2014).
- [21] F. Rose, M. O. Goerbig, and F. Piechon, *Physical Review B* **88**, 125438 (2013).
- [22] X. Li, F. Zhang, and Q. Niu, *Physical Review Letters* **110**, 066803 (2013).
- [23] A. Kormanyos, P. Rakytá, and G. Burkard, *New Journal of Physics* **17**, 103006 (2015).
- [24] Z. F. Wang, J. Shan, and K. F. Mak, *Nature Nanotechnology* **12**, 144 (2017).
- [25] T. Ando and Y. Uemura, *Journal of the Physical Society of Japan* **36**, 959 (1974).
- [26] R. R. Gerhardt, *Physica Status Solidi B* **245**, 378 (2008).
- [27] R. Pisoni, Z. J. Lei, P. Back, M. Eich, H. Overweg, Y. Lee, K. Watanabe, T. Taniguchi, T. Ihn, and K. Ensslin, *Applied Physics Letters* **112**, 123101 (2018).
- [28] Only part of the results from the original publication has been reproduced. An alternative set of data would be the same plot with the E_z/E_c values downshifted by 2.
- [29] K. S. Novoselov, A. K. Geim, S. V. Morozov, D. Jiang, M. I. Katsnelson, I. V. Grigorieva, S. V. Dubonos, and A. A. Firsov, *Nature* **438**, 197 (2005).
- [30] Y. Zhang, Y.-W. Tan, H. L. Stormer, and P. Kim, *Nature* **438**, 201 (2005).

High magnetic field spin-valley-split Shubnikov–de Haas oscillations in a WSe₂ monolayer

Supplemental Material

Banan Kerdi ^{1,*} Mathieu Pierre ¹ Robin Cours,² Bénédicte Warot-Fonrose ² Michel Goiran,¹ and Walter Escoffier^{1,†}

¹LNCMI, Université de Toulouse, CNRS, INSA, UPS, EMFL, 31400 Toulouse, France

²CEMES, Université de Toulouse, CNRS, 31055 Toulouse, France

I. Magneto-resistance oscillations versus filling factor

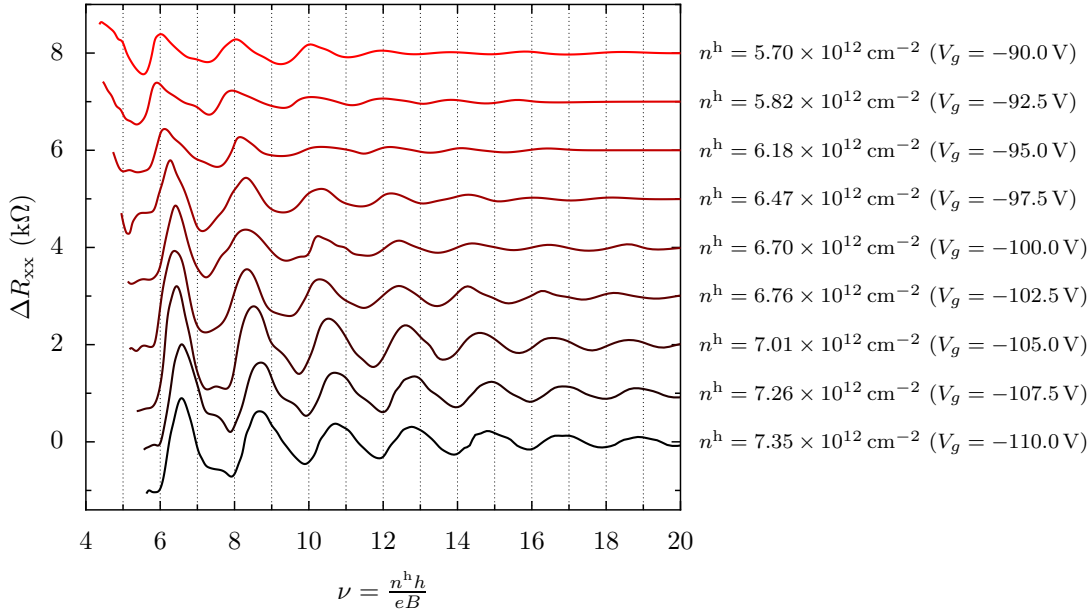


FIG. 1. Experimental magneto-resistance oscillations (background subtracted) at $T = 4.2$ K plotted versus filling factor $\nu = \frac{n^h h}{eB}$. The curves are successively offset by $1 \text{ k}\Omega$ for clarity. The carrier density was extracted from the fitting procedure described in the main text.

* banan.kerdi@lncmi.cnrs.fr

† walter.escoffier@lncmi.cnrs.fr

II. Additional fitting of the experimental magneto-resistance oscillations

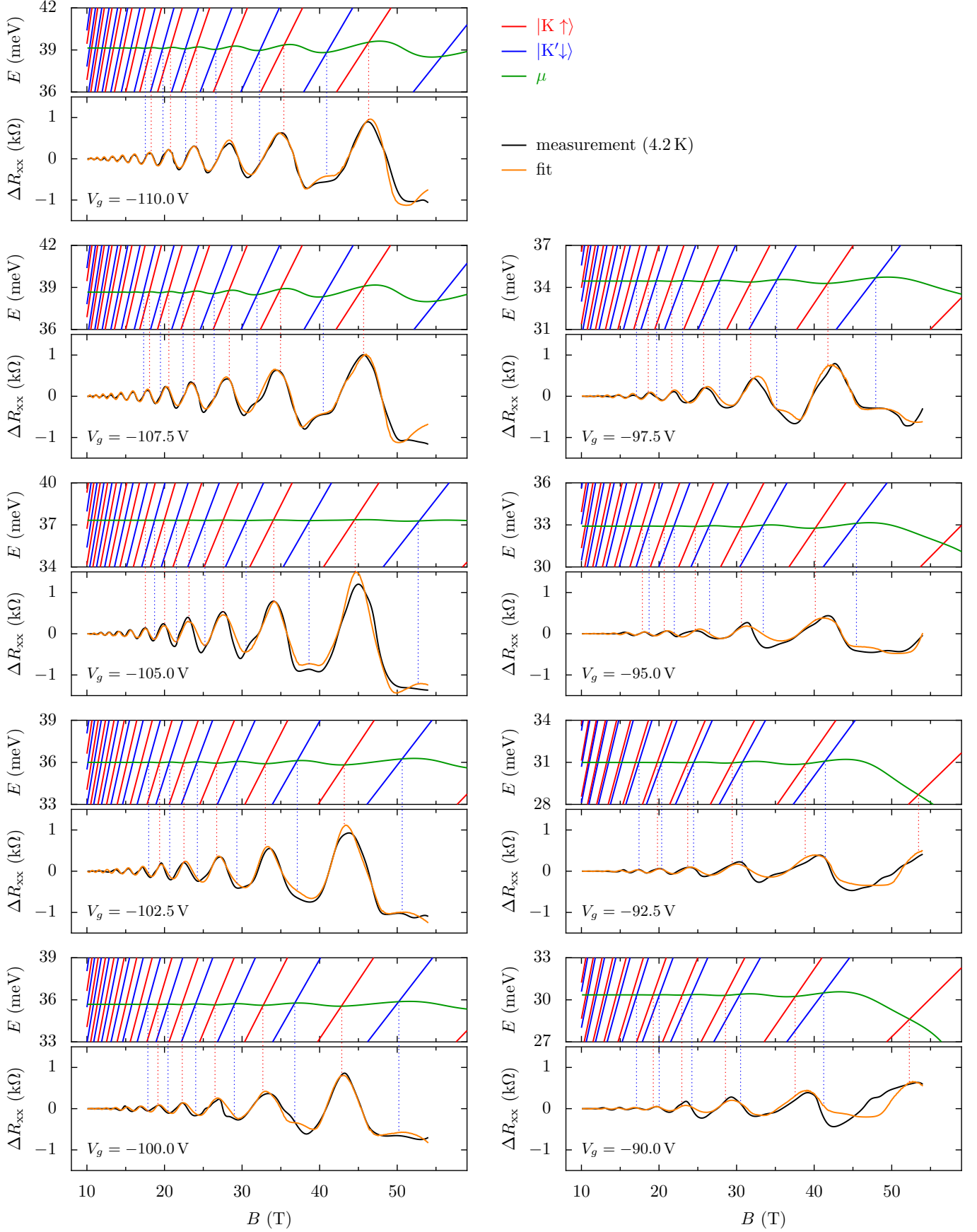


FIG. 2. Fit of the magneto-resistance oscillations and corresponding LL structure and chemical potential for all measurements at gate voltages between -110 and -90 V. The fitting parameters are given in Table I.

V_g (V)	-110	-107.5	-105	-102.5	-100	-97.5	-95	-92.5	-90
n^h ($\times 10^{12} \text{ cm}^{-2}$)	7.35	7.26	7.01	6.76	6.70	6.47	6.18	5.82	5.70
E_z/E_c	3.37	3.36	3.49	3.56	3.55	3.62	3.66	3.83	3.75
μ^h ($\text{cm}^2 \text{ V}^{-1} \text{ s}^{-1}$)	2400	2400	2400	2400	2200	1600	1400	1200	1300

TABLE I. Hole density, E_z/E_c ratio, and zero-field mobility obtained from the fit of the experimental quantum oscillations shown in Fig. 2.

III. Comparison of the hole carrier density extracted from the fit and the plane capacitor model

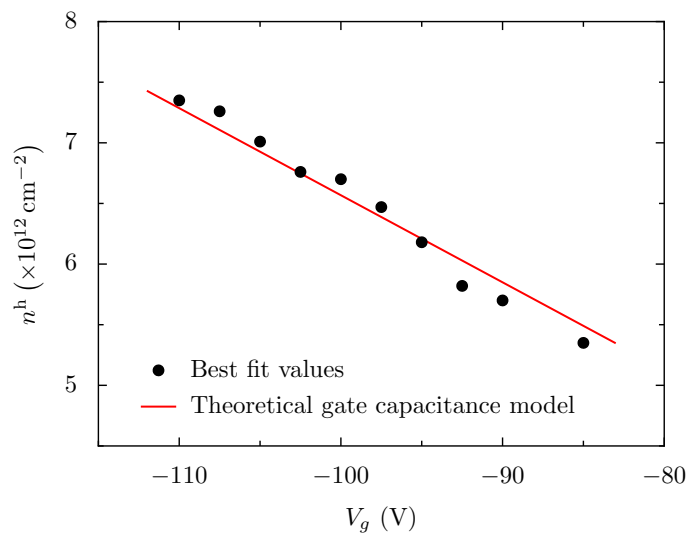


FIG. 3. The hole carrier density extracted from the fitting of the magneto-resistance oscillations is compared to its theoretical evolution with back-gate voltage, based on the calculation of the back-gate capacitance with the plane capacitor model, which gives $C_g = 11.5 \text{ nF/cm}^2$.

IV. Determination of the cyclotron mass

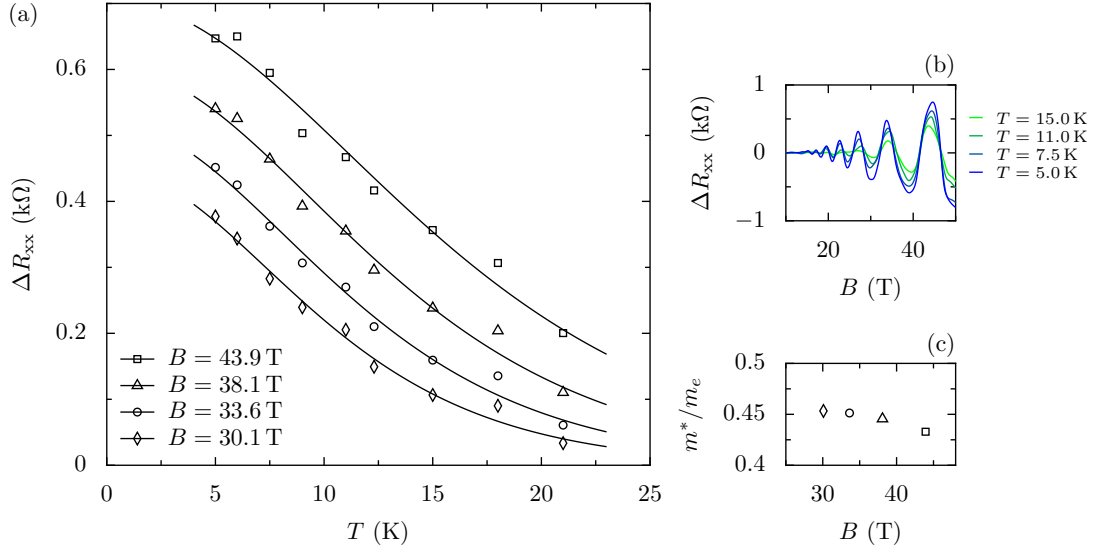


FIG. 4. (a) Amplitudes of the four highest magnetic field oscillations measured at for $V_g = -105$ V versus temperature. Their decay with temperature is fitted with the Lifshitz-Kosevich model: $\Delta R_{xx}(T) \propto x/\sinh(x)$ with $x = (2\pi^2 m^* k_B T)/(\hbar e B)$. (b) Corresponding magneto-resistance oscillation measurements (background subtracted) for selected temperatures. (c) Effective mass resulting from the fits shown in panel (a). We extract an effective mass $m^* = (0.45 \pm 0.04) \times m_e$, which confirms previous reports in the literature for WSe₂ monolayers.